

ωN scattering length from ω photoproduction on the proton near the threshold

T. Ishikawa,^{1, a} H. Fujimura,^{1, b} H. Fukasawa,¹ R. Hashimoto,^{1, c} Q. He,^{1, d} Y. Honda,¹ A. Hosaka,^{2, 3} T. Iwata,⁴ S. Kaida,¹ J. Kasagi,¹ A. Kawano,⁵ S. Kuwasaki,¹ K. Maeda,⁶ S. Masumoto,⁷ M. Miyabe,¹ F. Miyahara,^{1, e} K. Mochizuki,¹ N. Muramatsu,¹ A. Nakamura,¹ S.X. Nakamura,⁸ K. Nawa,¹ S. Ogushi,¹ Y. Okada,¹ K. Okamura,¹ Y. Onodera,¹ K. Ozawa,⁹ Y. Sakamoto,⁵ M. Sato,¹ T. Sato,² H. Shimizu,¹ H. Sugai,^{1, f} K. Suzuki,^{1, g} Y. Tajima,⁴ S. Takahashi,¹ Y. Taniguchi,¹ Y. Tsuchikawa,^{1, h} H. Yamazaki,^{1, i} R. Yamazaki,¹ and H.Y. Yoshida⁴

¹Research Center for Electron Photon Science (ELPH),
Tohoku University, Sendai, Miyagi 982-0826, Japan

²Research Center for Nuclear Physics (RCNP), Osaka University, Ibaraki 567-0047, Japan

³Advanced Science Research Center, Japan Atomic Energy Agency (JAEA), Tokai 319-1195, Japan

⁴Department of Physics, Yamagata University, Yamagata 990-8560, Japan

⁵Department of Information Science, Tohoku Gakuin University, Sendai 981-3193, Japan

⁶Department of Physics, Tohoku University, Sendai 980-8578, Japan

⁷Department of Physics, University of Tokyo, Tokyo 113-0033, Japan

⁸University of Science and Technology of China, Hefei 230026, China

⁹Institute of Particle and Nuclear Studies, High Energy Accelerator Research Organization (KEK), Tsukuba 305-0801, Japan

Photoproduction of the ω meson on the proton has been experimentally studied near the threshold. The total cross sections are determined at incident energies ranging from 1.09 to 1.15 GeV. The 1/2 and 3/2 spin-averaged scattering length $a_{\omega p}$ and effective range $r_{\omega p}$ between the ω meson and proton are estimated from the shape of the total cross section as a function of the incident photon energy: $a_{\omega p} = \left(-0.97^{+0.16_{\text{stat}}+0.03_{\text{sys}}} \right) + i \left(0.07^{+0.15_{\text{stat}}+0.17_{\text{sys}}} \right)$ fm and $r_{\omega p} = \left(+2.78^{+0.68_{\text{stat}}+0.11_{\text{sys}}} \right) + i \left(-0.01^{+0.46_{\text{stat}}+0.07_{\text{sys}}} \right)$ fm, resulting in a repulsive force. The real and imaginary parts for $a_{\omega p}$ and $r_{\omega p}$ are determined separately for the first time. A small P -wave contribution does not affect the obtained values.

PACS numbers: 13.60.Le, 14.40.Be, 25.20.Lj

The structure of hadrons and dynamical hadron-mass generation are the most important subjects to be studied in the non-perturbative domain of quantum chromodynamics (QCD). The ω meson (ω) is one of the best established hadrons, and it is considered to give a short-ranged repulsive central force and a strong spin-orbit force between two nucleons (N s) [1]. Nevertheless, the fundamental properties of ω such as the interaction with N is not known yet due to the difficulties in realizing scattering experiments. Detailed information on ωN scattering would not only reveal highly excited nucleon resonances (N^*) but also have a strong relevance to the equation of state (EoS) describing the interior of neutron stars [2]. Gravitational wave observations just have begun to provide information on EoS [3].

The low-energy ωN scattering is characterized by the scattering length $a_{\omega N}$ and effective range $r_{\omega N}$ through an effective-range expansion of the S -wave phase shift $\delta(p)$:

$$p \cot \delta(p) = \frac{1}{a_{\omega N}} + \frac{1}{2} r_{\omega N} p^2 + O(p^4), \quad (1)$$

where p denotes the momentum of ω in the ωN center-of-mass (CM) frame. A positive (negative) $\text{Re } a_{\omega N}$ gives attraction (repulsion), and a positive $\text{Im } a_{\omega N}$ corresponds to the absorption to another channel such as $\omega N \rightarrow \pi N$. The $r_{\omega N}$ provides the momentum dependence of the interaction. Recently, the A2 collaboration at the Mainz MAMI facility has reported $|a_{\omega N}| = 0.82 \pm 0.03$ fm,

which is extracted from ω photoproduction on the proton ($\gamma p \rightarrow \omega p$) near the threshold assuming a vector meson dominance (VMD) model [4]. The obtained value is a combination of two independent S -wave scattering lengths with total spins of 1/2 and 3/2. The unknown sign of $a_{\omega N}$ leaves the naive question of whether low-energy ωN scattering is repulsive or attractive.

Theoretically estimated values of $a_{\omega N}$ are scattered in a wide range from attractive to repulsive ones. The effective Lagrangian approach based on chiral symmetry gives an attractive value of $a_{\omega N} = +1.6 + i0.30$ fm [5]. A QCD sum-rule analysis provides a weakly attractive value of $a_{\omega N} = +0.41 \pm 0.05$ fm [6]. The coupled-channel unitary approach gives repulsive values of $a_{\omega N}^{(1/2)} = -0.45 + i0.31$ fm and $a_{\omega N}^{(3/2)} = -0.43 + i0.15$ fm for the two total spins, giving a spin-averaged value of $a_{\omega N} = -0.44 + i0.20$ fm [7]. The coupled-channel analysis of ω production in pion and photo-induced reactions gives a very weakly repulsive value of $a_{\omega N} = -0.026 + i0.28$ fm [8]. The dynamical coupled-channel analysis resulted in $a_{\omega N}^{(1/2)} = 0.0454 + i0.0695$ fm and $a_{\omega N}^{(3/2)} = -0.180 + i0.0597$ fm, giving a repulsive spin-averaged value¹ of $a_{\omega N} = -0.135 + i0.0630$ fm [9]. Nei-

¹ We adopt $a_{\omega N} = (1/3)a_{\omega N}^{(1/2)} + (2/3)a_{\omega N}^{(3/2)}$ for the spin average using the convention of Lutz *et al.* [7, 8].

ther the coupled-channel analyses nor the VMD analysis by the A2 collaboration incorporates the finite width of ω in the final state.

To determine the low-energy ωN scattering parameters $a_{\omega N}$ and $r_{\omega N}$ experimentally, we investigate the $\gamma p \rightarrow \omega p$ reaction very close to the reaction threshold. Several collaborations have already measured the total cross sections near the threshold using the $\omega \rightarrow \pi^+\pi^-\pi^0$ decay mode (SAPHIR [10] and CLAS [11] collaborations), and the $\omega \rightarrow \pi^0\gamma$ decay mode (CBELSA/TAPS [12] and A2 [4] collaborations). Currently, the data points for the total cross section near the threshold ($E_\gamma \lesssim 1.2$ GeV), where the S -wave ωN contribution is dominant, are not enough for determining $a_{\omega N}$ and $r_{\omega N}$ from the shape of the total cross section as a function of the incident energy (excitation function) through ωN rescattering in the final-state interaction. We have measured ten data points of the total cross section at incident photon energies ranging from 1.09 to 1.15 GeV. The ω meson mainly decays in the $\omega \rightarrow \pi^0\pi^+\pi^-$ mode with a branching ratio of 89.2% [13]. It is, however, difficult to reproduce the background shapes in the $\pi^0\pi^+\pi^-$ invariant mass distributions measured with poor identification for charged particles [14]. Thus, we determined the cross sections using the $\omega \rightarrow \pi^0\gamma$ decay mode with a branching ratio of 8.40%. In this letter, we present $a_{\omega N}$ and $r_{\omega N}$ extracted from the shape of the excitation function for the $\gamma p \rightarrow \omega p$ reaction.

A series of meson photoproduction experiments were conducted [15] using the FOREST detector [16], which was installed on the second photon beamline [17] at the Research Center for Electron Photon Science (ELPH), Tohoku University, Japan. In the present experiments, bremsstrahlung photons were produced from 1.2-GeV circulating electrons in a synchrotron [18] by inserting a carbon thread (radiator) [17]. The photons collimated with two lead apertures of 10 and 25 mm in diameter located 4.2- and 12.9-m downstream from the radiator, respectively, were incident on a 45-mm thick liquid-hydrogen target located at the center of FOREST. The energies of the incident photons were analyzed up to 1.15 GeV by detecting the post-bremsstrahlung electrons with a photon-tagging counter, STB-Tagger II [17]. FOREST consists of three different electromagnetic calorimeters (EMCs): 192 undoped CsI crystals, 252 lead scintillating-fiber modules, and 62 lead glasses. A plastic-scintillator hodoscope (PSH) is placed in front of each EMC to identify charged particles. FOREST covers a solid angle of $\sim 88\%$ in total. The typical photon-tagging rate was 20 MHz, and the photon transmittance (the so-called tagging efficiency) was $\sim 53\%$ [17]. The trigger condition of the data acquisition (DAQ), which required for an event to have more than one final-state particles in coincidence with a photon-tagging signal [16], was the same as that in Ref. [19]. The total number of collected events in DAQ was 1.79×10^9 . The average trigger rate was 1.6 kHz, and

the average DAQ efficiency was 80%.

Event selection was made for the $\gamma p \rightarrow \pi^0 \gamma p \rightarrow \gamma \gamma \gamma p$ reaction. At first, events containing three neutral particles and a charged particle were selected. The time difference between every 2 neutral EMC clusters out of 3 was required to be less than thrice that of the time resolution for the difference. The two neutral EMC clusters giving the $\gamma\gamma$ invariant mass ranging from 50 to 220 MeV were selected, and the other EMC cluster was required to have an energy higher than 200 MeV. The charged particles were detected with the forward PSH. Further selection was made by applying a kinematic fit with five constraints: energy and three-momentum conservation, and $\gamma\gamma$ invariant mass being the π^0 mass. The momentum of the charged particle was obtained from the time delay assuming that the charged particle had proton mass. Events for which the χ^2 probability was higher than 0.1 were selected. When the number of combinations was more than 1 in an event, the combination with the minimum χ^2 was adopted. Sideband-background subtraction was performed for accidental-coincidence events detected in STB-Tagger II and FOREST.

All the data for incident energies above 1.09 GeV ($E_\gamma = 1.09\text{--}1.15$ GeV) are divided into ten bins (every bin includes 4 photon-tagging channels), and 10 angular bins of the $\pi^0\gamma$ emission angle $\cos\theta$ in the γp -CM frame. The typical $\pi^0\gamma$ invariant mass ($M_{\pi\gamma}$) distributions are shown in Fig. 1. Each $M_{\pi\gamma}$ distribution shows a prominent peak with a centroid of ~ 0.78 GeV, and has a broad background contribution in the lower side. This background contribution is well reproduced by a Monte-Carlo (MC) simulation based on Geant4 [20] for the $\gamma p \rightarrow \pi^0\pi^0p \rightarrow \gamma\gamma\gamma\gamma p$ reaction, where 1 γ out of 4 is not detected with FOREST. In the simulation, the five-fold differential cross sections are assumed to be the same

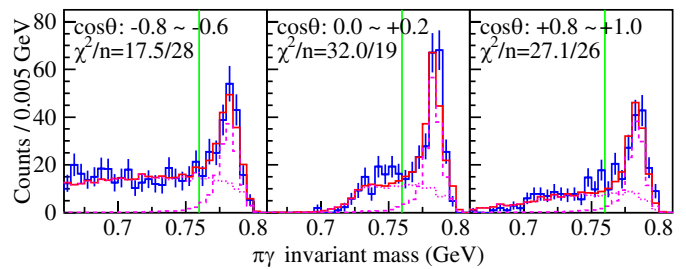


FIG. 1. Typical $M_{\pi\gamma}$ distributions for the highest incident energy group ($E_\gamma = 1.144\text{--}1.149$ GeV). In each panel, the histogram (blue) shows the experimentally obtained $M_{\pi\gamma}$ distribution, and the solid curve (red) shows the sum of the $M_{\pi\gamma}$ distributions obtained in the simulation for the $\gamma p \rightarrow \omega p \rightarrow \pi^0 \gamma p$ and $\gamma p \rightarrow \pi^0 \pi^0 p$ reactions. The dashed (magenta) and dotted (cyan) curves show these contributions. The angular region of π^0 emission in the γp -CM frame is described in each panel. The vertical lines show the lower limit $M_{\pi\gamma} = 0.76$ GeV for selecting the ω produced events.

as those provided by the 2-PION-MAID calculation [21]. The $M_{\pi\gamma}$ distributions for the $\gamma p \rightarrow \pi^0\pi^0p$ reaction are also plotted in Fig. 1 where the same analysis is applied as for the $\gamma p \rightarrow \pi^0\gamma p$ reaction.

The $M_{\pi\gamma}$ distributions for the $\gamma p \rightarrow \omega p \rightarrow \pi^0\gamma p \rightarrow \gamma\gamma\gamma p$ and $\gamma p \rightarrow \pi^0\pi^0p \rightarrow \gamma\gamma\gamma p$ reactions in the MC simulation are fitted to the measured $M_{\pi\gamma}$ distribution for each emission-angle incident-energy bin only by changing the normalization coefficients. Here, the events are generated according to the pure phase space for the $\gamma p \rightarrow \omega p$ reaction. The number of the ω produced events N_ω is estimated for $M_{\pi\gamma} \geq 0.76$ GeV after subtracting the background $\gamma p \rightarrow \pi^0\pi^0p$ contribution for each bin. The angular differential cross section is obtained from $N_\omega(\cos\theta)$ as

$$\frac{d\sigma}{d\Omega} = \frac{N_\omega(\cos\theta)}{2\pi\Delta\cos\theta N_\gamma N_\tau \eta_{\text{acc}}(\cos\theta) \text{BR}(\omega \rightarrow \gamma\gamma\gamma)}, \quad (2)$$

with the incident photon flux including the DAQ efficiency correction N_γ , the number of target protons N_τ , the multiplication of branching ratios for the $\omega \rightarrow \pi^0\gamma$ and $\pi^0 \rightarrow \gamma\gamma$ decays $\text{BR}(\omega \rightarrow \gamma\gamma\gamma)$, and the detector acceptance calculated in the simulation $\eta_{\text{acc}}(\cos\theta)$, where $\Delta\cos\theta = 0.2$. Fig. 2 shows the typical $d\sigma/d\Omega$ distributions. The systematic uncertainty of $d\sigma/d\Omega$ is also given in Fig. 2. It includes the uncertainty of event selection in the kinematic fit, that of counting N_ω due to the $M_{\pi\gamma}$ threshold, that of acceptance owing to the uncertainties of the $d\sigma/d\Omega$ distributions for event generation in the simulation, that of detection efficiency of protons, and that of normalization resulting from N_τ and N_γ .

Every $d\sigma/d\Omega$ distribution shows a slight increase with increase of $\cos\theta$. A finite P -wave amplitude must produce asymmetric behavior of the angular distribution

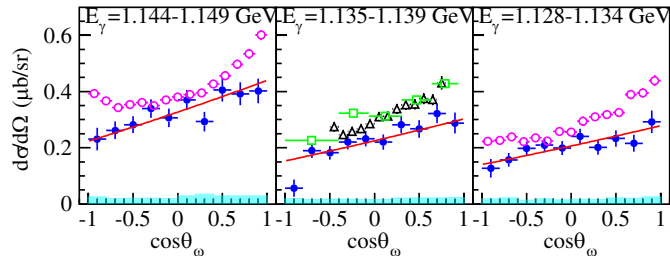


FIG. 2. Typical angular differential cross sections $d\sigma/d\Omega$ as a function of the ω emission angle $\cos\theta$ in the γp -CM frame. The range of the incident photon energies is described in each panel. The filled circles (blue) represent the measured $d\sigma/d\Omega$ in this work. The shaded areas represent the systematic uncertainties of $d\sigma/d\Omega$ s. The solid curves show the fitted distribution with a P -wave contribution of $\sigma_{\text{max}}^P/5$ (see text). The $d\sigma/d\Omega$ results from SAPHIR [10], CLAS [11], and A2 [4] collaborations are depicted by open boxes (green), open triangles (black), and open circles (magenta), respectively. The photon-energy coverages are 25, 18, 15, and ~ 4.5 MeV in SAPHIR, CLAS, A2, and our results, respectively.

through the interference with the S -wave amplitude although the S -wave contribution is expected to be dominant near the threshold. The measured $d\sigma/d\Omega$ s in this work are somewhat lower than the world available data. The obtained $d\sigma/d\Omega$ depends on the incident-energy coverage because the cross section increases rapidly as the incident energy goes up. The bin size of the incident energy is ~ 4.5 MeV in our results, while that for the SAPHIR [10] data is 25 MeV, 18 MeV (CLAS [11]), and 15 MeV (A2 [4]), respectively. In Fig. 2, the angular distribution obtained by the A2 collaboration at $E_\gamma \simeq 1.14$ GeV shows a shape being concave upward, suggesting a P -wave contribution, although any significant slope changes are not observed in this work. Apparently this deviation comes from the relative difference of centroid photon-tagging energies by a few MeV. The uncertainty of the centroid photon-tagging energies is estimated to be 0.3%, which corresponds to 3–4 MeV. A calibration difference of photon-tagging energies needs to be incorporated in the estimation of the systematic uncertainty for $a_{\omega p}$ and $r_{\omega p}$.

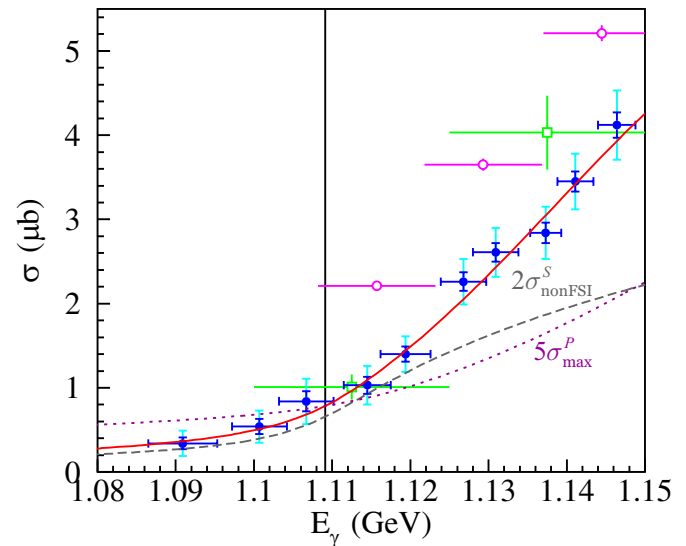


FIG. 3. Total cross section σ as a function of E_γ . The filled circles (blue) represent the measured σ in this work. Each horizontal bar indicates the incident-energy coverage. Each short vertical bar (blue) represents the statistical error of σ , and the connected bars (cyan) indicate the upper- and lower-side systematic error of σ . The vertical line (black) shows E_γ corresponding to the reaction threshold for production of ω having a mass of the centroid. The solid curve (red) shows the calculated excitation function with the parameters: $a_{\omega p} = -0.97 + i0.07$ fm and $r_{\omega p} = +2.78 - i0.01$ fm. The dashed curves (gray) show $2\sigma_{\text{nonFSI}}^S$ where σ_{nonFSI}^S denotes the excitation function with $a_{\omega p} = 0$ fm and $r_{\omega p} = 0$ fm. The dotted curve (purple) shows $5\sigma_{\text{max}}^P$ where σ_{max}^P stands for the upper limit of the P -wave contribution. The σ results from SAPHIR [10] and A2 [4] collaborations are depicted by open boxes (green) and open circles (magenta), respectively.

The total cross section σ is obtained by integrating $d\sigma/d\Omega$ s all over the ten emission-angle bins:

$$\sigma = \sum 2\pi\Delta \cos\theta \frac{d\sigma}{d\Omega}. \quad (3)$$

Fig. 3 shows σ as a function of the incident photon energy. The excitation function shows a monotonic increase, and finite yields are observed below the threshold E_γ^{thr} for production of ω having the centroid mass. The obtained cross sections show a systematic deviation from the world available data. The uncertainty of tagging-energy determination (0.3%) for the incident photon beam may account for the deviation.

We determine $a_{\omega p}$ and $r_{\omega p}$ from the shape of the excitation function. We evaluate the excitation function for the $\gamma p \rightarrow \omega p$ reaction using a model with final-state ωp interaction (FSI) based on the Lippmann-Schwinger equation. We assume that the S -wave contribution is dominant at $E_\gamma = 1.09\text{--}1.15$ GeV. The total cross section for a fixed ω mass M and γp -CM energy W can be calculated using a transition amplitude $T_{\gamma p \rightarrow \omega p}(W, M)$:

$$\sigma_0(W, M) = \frac{1}{16\pi W^2} \frac{p(W, M)}{k} |T_{\gamma p \rightarrow \omega p}(W, M)|^2, \quad (4)$$

$$\begin{aligned} & \langle \omega p(p) | T_{\gamma p \rightarrow \omega p} | \gamma p(k) \rangle \\ &= \langle \omega p(p) | V_{\gamma p \rightarrow \omega p} | \gamma p(k) \rangle + \int \langle \omega p(p) | T_{\omega p \rightarrow \omega p} | \omega p(q) \rangle \frac{\delta^3(\vec{q} - \vec{q}')}{W - H_0 + i\epsilon} \langle \omega p(q') | V_{\gamma p \rightarrow \omega p} | \gamma p(k) \rangle d\vec{q} d\vec{q}' \\ &\simeq \left[1 + 8\pi\mu \langle \omega p(p) | T_{\omega p \rightarrow \omega p} | \omega p(p) \rangle \int \frac{d\vec{q}}{p^2 - q^2 + i\mu\Gamma_\omega} \exp\left(-\frac{q^2}{\Lambda^2}\right) \right] \langle \omega p(p) | V_{\gamma p \rightarrow \omega p} | \gamma p(k) \rangle, \end{aligned} \quad (7)$$

where H_0 stands for the free Hamiltonian for the final-state ωp , and μ denotes a reduced mass between ω (with a mass of M) and the proton. Here, we use a cut-off

where k and p denote the momenta of an initial- and a final-state particles, respectively, in the γp -CM frame. The total cross section σ as a function of E_γ is obtained by averaging $\sigma_0(W(E_\gamma), M)$ over available ω masses:

$$\sigma(E_\gamma) = \int_{m_{\pi^0}}^{W(E_\gamma) - m_p} \sigma_0(W(E_\gamma), M) L_\omega(M) dM, \quad (5)$$

where the probability $L_\omega(M)$ stands for a Breit-Wigner function with a centroid of $M_\omega = 782.65$ MeV and a width of $\Gamma_\omega = 8.49$ MeV [13].

The $T_{\gamma p \rightarrow \omega p}$ is expressed by

$$T_{\gamma p \rightarrow \omega p} = V_{\gamma p \rightarrow \omega p} + T_{\omega p \rightarrow \omega p} G_{\omega p \rightarrow \omega p} V_{\gamma p \rightarrow \omega p}, \quad (6)$$

where $T_{\omega p \rightarrow \omega p}$ stands for the ωp scattering amplitude, $G_{\omega p \rightarrow \omega p}$ denotes the ωp propagator, and $V_{\gamma p \rightarrow \omega p}$ is the production amplitude without FSI. We evaluate the matrix element for $T_{\gamma p \rightarrow \omega p}$ with on-shell approximations for $T_{\omega p \rightarrow \omega p}$ and $V_{\gamma p \rightarrow \omega p}$, and introduce a Gaussian form factor in the integration of $G_{\omega p \rightarrow \omega p}$. This leads the matrix element of $T_{\gamma p \rightarrow \omega p}$ to the equation:

parameter $\Lambda = 0.8$ GeV/ c . The $\langle \omega p(p) | T_{\omega p \rightarrow \omega p} | \omega p(p) \rangle$ is given by $a_{\omega p}$ and $r_{\omega p}$:

$$\langle \omega p(p) | T_{\omega p \rightarrow \omega p} | \omega p(p) \rangle = -\frac{1}{(2\pi)^2 \mu} \left(\frac{1}{a_{\omega p}} + \frac{1}{2} r_{\omega p} p^2 - ip \right)^{-1}. \quad (8)$$

The $\langle \omega p(p) | V_{\gamma p \rightarrow \omega p} | \gamma p(k) \rangle$ is assumed to be a constant value of 1 in the incident-energy region of interest.

The dashed curve (gray) in Fig. 3 shows the excitation function σ_{nonFSI}^S with $a_{\omega p} = 0$ fm and $r_{\omega p} = 0$ fm corresponding to non FSI condition, which does not reproduce the experimental data. FSI is necessary and the optimal set of $a_{\omega p}$ and $r_{\omega p}$ are determined to reproduce the experimentally obtained cross section data.

The χ^2 corresponding to the reproducibility is defined as

$$\chi^2 = \sum_{i=1}^{10} \frac{(\sigma_i - \alpha Y_i)^2}{\left(\delta\sigma_i^{(\text{stat})} \right)^2 + \left(\delta\sigma_i^{(\text{syst})} \right)^2}, \quad (9)$$

where σ_i , $\delta\sigma_i^{(\text{stat})}$, $\delta\sigma_i^{(\text{syst})}$, and Y_i denote the measured total cross section, its statistical error, its systematic error, and the yield estimated in Eq. (5) by taking the coverage of incident energies into account, respectively, for the i -th incident-energy bin. The coefficient α for the overall normalization is determined to

minimize χ^2 for each parameter set. The deduced values are $a_{\omega p} = (-0.97^{+0.16+0.03}_{-0.16-0.00}) + i(0.07^{+0.15+0.17}_{-0.14-0.09})$ fm and $r_{\omega p} = (+2.78^{+0.68+0.11}_{-0.54-0.13}) + i(-0.01^{+0.46+0.07}_{-0.50-0.00})$ fm. The first and second errors for each parameter refer to the statistical and systematic uncertainties, respectively. The systematic uncertainty is estimated from that of the mean incident energy ($\pm 0.3\%$) for each photon-tagging bin. The solid (red) curve in Fig. 3 shows the excitation function with the optimal parameters. No significant changes are observed for the $a_{\omega p}$ and $r_{\omega p}$ parameters when we shift the incident photon energies by $\pm 0.3\%$. This is because these parameters are primarily determined by the shape of the excitation function.

The parameters may be somewhat affected by the adopted Λ . We also determine $a_{\omega p}$ and $r_{\omega p}$ for $\Lambda = 0.6$ and 1.0 GeV/ c . The obtained values are summarized in Table I. Although $|\text{Re } a_{\omega p}|$ and $|\text{Im } a_{\omega p}|$ become larger with decrease of Λ , changes of $a_{\omega p}$ and $r_{\omega p}$ are not significant among the realistic Λ values.

The asymmetric behavior of the angular distribution mainly comes from interference between S - and P -wave contributions. The dotted curve (magenta) in Fig. 3 shows the shape of the P -wave excitation function where $\sigma_0^P(W, M) \propto p^3/k$ is assumed. The finite width of ω makes the P -wave excitation function rather flat, and the P -wave contribution does not explain the gap at higher incident energies between the data and calculation without FSI. We also fit the excitation function adding a P -wave contribution to the experimental data by fixing $\text{Im } r_{\omega p} = 0$ fm, obtaining the values given in Table I. The optimal coefficient to the P -wave contribution is 0, and the P -wave total cross section is 0 with an error of σ_{max}^P . The dotted curve in Fig. 3 corresponds to $5\sigma_{\text{max}}^P$. The asymmetric behavior in the angular distribution shown in Fig. 2 requires a finite P -wave contribution. The solid curve in Fig. 2 corresponds to a solution under the condition that the P -wave contribution in σ is $\sigma_{\text{max}}^P/5$. We can conclude that the P -wave contribution in σ is negligibly small in determination of $a_{\omega p}$ and $r_{\omega p}$.

We have assumed that $V_{\gamma p \rightarrow \omega p}$ is constant since the coverage of incident energies is narrow ($E_\gamma = 1.09$ – 1.15 GeV) for several overlapping N^* s with a very wide width. We deduce the scattering parameters with $\text{Im } r_{\omega p} = 0$ fm by assuming a single N^* contribution $D_{13}(1700)$ as an extreme condition:

$$V_{\gamma p \rightarrow \omega p} \propto (W^2 - M_{N^*}^2 + iM_{N^*}\Gamma_{N^*})^{-1} \quad (10)$$

where $M_{N^*} = 1.7$ GeV and $\Gamma_{N^*} = 0.2$ GeV [13]. The change of each parameter from the constant $V_{\gamma p \rightarrow \omega p}$ is not significant.

Fig. 4 shows the real and imaginary parts of $1/2$ and $3/2$ spin-averaged $a_{\omega p}$ obtained by assuming a constant $V_{\gamma p \rightarrow \omega p}$ in this work together with the previously obtained values. It is consistent with $|a_{\omega p}| = 0.82 \pm 0.03$ fm given by the A2 collaboration [4]. The other values correspond to the theoretical predictions. The positive $\text{Re } a_{\omega p}$

value, giving an attraction, is rejected at a confidence level higher than 99.9%. The repulsion is found to be much stronger than the πN ones, and no bound or virtual state is expected for ωN . Slightly attractive ω -nucleus (ωA) interactions are reported with potential depths at normal nuclear density of $-42 \pm 17 \pm 20$ MeV [22] and $-15 \pm 35 \pm 20$ MeV [23] from ω photoproduction from nuclei. The measurement of ω line shape shows a decrease of ω mass by $9.2\% \pm 0.2\%$ (corresponding to ωA attraction) without any in-medium broadening [24, 25]. The relation between strong ωN repulsion and ωA attraction would be a subject of future discussions taking into consideration spin-dependent terms, higher partial waves, and partial restoration of chiral symmetry.

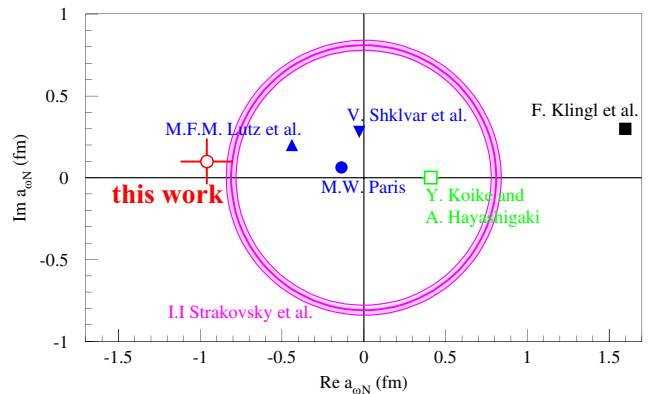


FIG. 4. Real and imaginary parts of spin-averaged $a_{\omega N}$ obtained in this work (red). The donut (magenta) represents the experimentally obtained $|a_{\omega N}|$ using a VMD model [4]. Other markers indicate $a_{\omega N}$ s obtained in the theoretical works on an effective Lagrangian approach [5] (black), a QCD sum-rule analysis [6] (green), coupled-channel analyses [7–9] (blue).

In summary, the total cross sections have been measured for the $\gamma p \rightarrow \omega p$ reaction near the threshold. The ω is identified through the $\omega \rightarrow \pi^0 \gamma$ decay. The spin-averaged scattering length $a_{\omega p}$ and effective range $r_{\omega p}$ between the ω and proton are estimated from the excitation function at incident photon energies ranging from 1.09 to 1.15 GeV: $a_{\omega p} = (-0.97^{+0.16+0.03}_{-0.16-0.00}) + i(0.07^{+0.15+0.17}_{-0.14-0.09})$ fm and $r_{\omega p} = (+2.78^{+0.68+0.11}_{-0.54-0.13}) + i(-0.01^{+0.46+0.07}_{-0.50-0.00})$ fm. The real and imaginary parts for $a_{\omega p}$ and $r_{\omega p}$ are determined separately for the first time. A small P -wave contribution does not affect the obtained values. The positive $\text{Re } a_{\omega p}$ value indicates repulsion.

The authors express gratitude to the ELPH accelerator staff for stable operation of the accelerators in the FOREST experiments. They acknowledge Mr. Kazue Matsuda, Mr. Ken'ichi Nanbu, and Mr. Ikuro Nagasawa for their technical assistance in the FOREST experiments. They received help at the early stage of this work from Dr. Hiroyuki Kamano. They also thank Prof. Igor I. Strakovsky for providing all the available

TABLE I. Deduced scattering parameters $a_{\omega p}$ and $r_{\omega p}$ for several conditions. The second, third, fourth lines show the results for different Λ cut-off parameters. The fifth line corresponds to the result with taking the P -wave contribution into account where $\text{Im } r_{\omega p}$ is fixed at 0 fm. The sixth line represents the result with the assumption that the energy dependence of the ω production amplitude is express by a single N^* resonance as an extreme case.

parameters	Re $a_{\omega p}$ (fm)	Im $a_{\omega p}$ (fm)	Re $r_{\omega p}$ (fm)	Im $r_{\omega p}$ (fm)
$\Lambda = 0.8 \text{ GeV}/c$	$-0.97^{+0.16+0.03}_{-0.16-0.00}$	$+0.07^{+0.15+0.17}_{-0.14-0.09}$	$+2.78^{+0.68+0.11}_{-0.54-0.13}$	$-0.01^{+0.46+0.07}_{-0.50-0.00}$
$\Lambda = 0.6 \text{ GeV}/c$	$-1.11^{+0.14+0.03}_{-0.16-0.02}$	$+0.12^{+0.17+0.15}_{-0.17-0.11}$	$+2.78^{+0.81+0.04}_{-0.57-0.11}$	$-0.00^{+0.44+0.11}_{-0.57-0.13}$
$\Lambda = 1.0 \text{ GeV}/c$	$-0.89^{+0.16+0.01}_{-0.18-0.00}$	$+0.04^{+0.14+0.13}_{-0.12-0.08}$	$+2.78^{+0.62+0.13}_{-0.51-0.09}$	$+0.01^{+0.47+0.03}_{-0.50-0.05}$
P -wave contribution	$-0.96^{+0.16+0.03}_{-0.16-0.01}$	$+0.10^{+0.14+0.14}_{-0.14-0.11}$	$+2.85^{+0.77+0.10}_{-0.53-0.15}$	0.00
single N^* contribution	$-0.87^{+0.15+0.04}_{-0.12-0.02}$	$+0.22^{+0.14+0.11}_{-0.12-0.11}$	$+2.69^{+0.62+0.06}_{-0.55-0.12}$	$-0.04^{+0.48+0.04}_{-0.69-0.14}$

numerical values of cross sections for the $\gamma p \rightarrow \omega p$ reaction. They are grateful to Prof. Mark W. Paris for giving us the numerical values on the total cross sections of a single partial wave. One of the authors (TI) expresses heartfelt gratitude to Dr. Shuntaro Sakai for several useful conversations. This work was supported in part by the Ministry of Education, Culture, Sports, Science and Technology, Japan (MEXT) and Japan Society for the Promotion of Science (JSPS) through Grants-in-Aid for Specially Promoted Research No. 19002003, for Scientific Research (A) Nos. 24244022 and 16H02188, for Scientific Research (B) Nos. 17340063 and 19H01902, for Scientific Research (C) No. 26400287, and for Scientific Research on Innovative Areas Nos. 18H05407 and 19H05141.

^a Corresponding author: ishikawa@ins.tohoku.ac.jp

^b Present address: Department of Physics, Wakayama Medical University, Wakayama 641-8509, Japan

^c Present address: Institute of Materials Structure Science (IMSS), KEK, Tsukuba 305-0801, Japan

^d Present address: Department of Nuclear Science and Engineering, Nanjing University of Aeronautics and Astronautics (NUAA), Nanjing 210016, China

^e Present address: Accelerator Laboratory, KEK, Tsukuba 305-0801, Japan

^f Present address: Gunma University Initiative for Advanced Research (GIAR), Maebashi 371-8511, Japan

^g Present address: The Wakasa Wan Energy Research Center, Tsuruga 914-0192, Japan

^h Present address: Department of Physics, Nagoya University, Nagoya 464-8602, Japan

ⁱ Present address: Radiation Science Center, KEK, Tokai 319-1195, Japan

[1] R. Machleidt, *Adv. Nucl. Phys.* **19**, 189 (1989).

[2] H. Shen, H. Toki, K. Oyamatsu, K. Sumiyoshi, *Nucl. Phys. A* **637**, 435 (1998).

[3] B. Abbott *et al.*, *Phys. Rev. Lett.* **119**, 161101 (2017).

[4] I.I. Strakovsky *et al.* (A2 collaboration at MAMI), *Phys. Rev. C* **91**, 045207 (2015).

[5] F. Klingl, T. Waas, and W. Weise, *Nucl. Phys. A* **650**,

299 (1999).

[6] Y. Koike, and A. Hayashigaki, *Prog. Theor. Phys.* **98**, 631 (1997).

[7] M.F.M. Lutz, Gy. Wolf, and B. Friman, *Nucl. Phys. A* **706**, 431 (2002); *ibid.* **765**, 495 (2006).

[8] V. Shklyar, H. Lenske, U. Mosel, and G. Penner, *Phys. Rev. C* **71**, 055206 (2005).

[9] M.W. Paris, *Phys. Rev. C* **79**, 025208 (2009).

[10] J. Barth *et al.* (SAPHIR collaboration), *Eur. Phys. J. A* **18**, 117 (2003).

[11] M. Williams *et al.* (CLAS collaboration), *Phys. Rev. C* **80**, 065208 (2009); *ibid.* **80**, 065209 (2009).

[12] A. Wilson *et al.* (CBELSA/TAPS collaboration), *Phys. Lett. B* **749**, 407 (2015).

[13] M. Tanabashi *et al.* (Particle Data Group), *Phys. Rev. D* **98**, 030001 (2018).

[14] R. Hashimoto *et al.*, *Few-Body Sys.* **54**, 1135 (2013).

[15] T. Ishikawa *et al.*, *JPS Conf. Proc.* **10**, 031001 (2016).

[16] T. Ishikawa *et al.*, *Nucl. Instrum. Meth. A* **832**, 108 (2016).

[17] T. Ishikawa *et al.*, *Nucl. Instrum. Meth. A* **622**, 1 (2010); T. Ishikawa *et al.*, *Nucl. Instrum. Meth. A* **811**, 124 (2016);

Y. Matsumura *et al.*, *Nucl. Instrum. Meth. A* **902**, 103 (2018);

Y. Obara *et al.*, *Nucl. Instrum. Meth. A* **922**, 108 (2019).

[18] F. Hinode *et al.*, *Proc. of 2005 Particle Accelerator Conference*, 2458 (2005).

[19] T. Ishikawa *et al.*, *Phys. Lett. B* **772**, 398 (2017);

T. Ishikawa *et al.*, *Phys. Lett. B* **789**, 413 (2019).

[20] S. Agostinelli *et al.*, *Nucl. Instrum. Meth. A* **506**, 250 (2003);

J. Allison *et al.*, *IEEE Trans. Nucl. Sci.* **53**, 270 (2006);

Geant4 website (<http://geant4.cern.ch/>).

[21] A. Fix, H. Arenhövel, *Euro. Phys. J. A* **25**, 115 (2005);

2-PION-MAID website (<https://maid.kph.uni-mainz.de/twopion/>).

[22] V. Metag *et al.*, *Prog. Part. Nucl. Phys.* **67**, 530 (2012);

V. Metag, *Hyperfine Interact.* **234**, 25 (2015).

[23] S. Friedrich *et al.* (CBELSA/TAPS collaboration), *Phys. Lett. B* **736**, 26 (2014).

[24] K. Ozawa *et al.*, *Phys. Rev. Lett.* **86**, 5019 (2001).

[25] M. Naruki *et al.*, *Phys. Rev. Lett.* **96**, 092301 (2006).